# Scattering bottleneck for spin dynamics in metallic helical antiferromagnetic dysprosium

M. C. Langner, S. Roy, A. F. Kemper, Y.-D. Chuang, S. K. Mishra, R. B. Versteeg, Y. Zhu, M. P. Hertlein, T. E. Glover, K. Dumesnil, and R. W. Schoenlein

Phys. Rev. B **92**, 184423 — Published 23 November 2015

DOI: 10.1103/PhysRevB.92.184423

# A Scattering Bottleneck for Spin Dynamics in Metallic Helical Antiferromagnetic Dysprosium

M.C. Langner,[1] S. Roy,[2] A. F. Kemper,[3] Y.-D. Chuang,[2] S. K. Mishra,[2] R. B. Versteeg,[2] Y. Zhu,[1] M.P. Hertlein,[2] T.E. Glover,[2] K. Dumesnil,[4] and R. W. Schoenlein[1]

[1]*Materials Science Division, Lawrence Berkeley National Laboratory, Berkeley, CA 94720, USA*
[2]*Advanced Light Source, Lawrence Berkeley National Laboratory, Berkeley CA 94720, USA*
[3]*Computational Sciences Division, Lawrence Berkeley National Laboratory, Berkeley CA 94720, USA*
[4]*Institut Jean Lamour (UMR CNRS 7198), Université de Lorraine, Vandoeuvre les Nancy, F-54500 France*

(Dated: November 4, 2015)

Ultrafast studies of magnetization dynamics have revealed fundamental processes that govern spin dynamics, and the emergence of time-resolved x-ray techniques has extended these studies to long-range spin structures that result from interactions with competing symmetries. By combining time-resolved resonant x-ray scattering and ultrafast magneto-optical Kerr studies, we show that the dynamics of the core spins in the helical magnetic structure occur on much longer time-scales than the excitation of conduction electrons in the Lanthanide metal Dy. The observed spin behavior differs markedly from that observed in the ferromagnetic phase of other Lanthanide metals or transition metals and is strongly dependent on temperature and excitation fluence. This unique behavior results from coupling of the real-space helical spin structure to the shape of the conduction electron Fermi surface in momentum space, which creates a bottleneck in spin scattering events that transfer the valence excitation to the core spins. The dependence of the dynamics on the inter-site interactions renders the helical ordering much more robust to perturbations than simple ferromagnetic or antiferromagnetic ordering, where dynamics are driven primarily by on-site interactions.

PACS numbers: 71.20.Eh, 78.70.Ck

## INTRODUCTION

The magnetic ground state of a material system is governed by the energetics of different spin and charge coupling such as exchange, dipolar, and spin-orbit interactions. Preferential destabilization of any one of the interactions can have profound effects on the net magnetic properties of the material. One way to manipulate the magnetic state is by applying external magnetic fields, which is often exploited in storage technologies to write information. With decreasing bit sizes and higher storage density, the long range switching fields are no longer favorable. A new paradigm is to use a controlled impulse to change the magnetization. An example of such an impulse is the strong electric field created by a femtosecond laser pulse. Intense research efforts seek to understand how fast and by what mechanism magnetic order is re-established after a femtosecond impulse destroys the long range order [1]. In particular, as the time-scale of the perturbation approaches the characteristic time of the exchange interaction ( 10-100 fs), the magnetic dynamics may enter a novel coupling regime where new exchange pathways may be established [2, 3]. These questions become increasingly complex in antiferromagnets where after the exchange is destabilized, a competition may arise between the inter- and intrasublattice ordering. Thus there may exist more than one pathway to establish the ground state and as a result, new transient phases may be observed.

Ultrafast optical measurements have been to used to explore fundamental spin-scattering mechanisms and control the magnetic state on femtosecond time-scales in systems with spatially uniform magnetic phases [1]. The advent of time-resolved x-ray scattering techniques has opened the door for similar studies in longer-range magnetic structures that result from magnetic interactions with competing symmetries. Lanthanide metals exhibit a variety of magnetic phases due to competition between spin-orbit coupling, magneto-elastic effects, and long-range exchange coupling mediated by the indirect RKKY (Ruderman-Kittel-Kasuya-Yoshida) interaction [4]. The nature of the exchange interaction creates a composite spin system comprised of closely coupled conduction and core electron spins that account for the majority of the magnetic moment. Helical or conically ordered phases, where the magnetic structure is characterized by a non-zero ordering wavevector, are created by competing symmetric and antisymmetric long-range exchange interactions, where the exchange interactions are determined by the spatial distribution of the conducting electron wave-functions.

Ultrafast demagnetization mechanisms have been previously explored in transition metal and lanthanide magnets using all-optical and x-ray dichroism techniques [1, 5–8]. These studies have focused on the angular momentum transfer between core spins, conducting spins, and lattice, and addressed the dynamics of the uniform ferromagnetic phase. Ultrafast optical pump/x-ray probe measurements reveal the coupling mechanisms between the constituent spin systems in Lanthanide magnets by observing the dynamics of core spins in response to excitation of conduction electrons responsible for the exchange interaction. An as yet unexplored aspect of these magnetic systems are the dynamics in the helical phase, where transiently altering the conduction electron distribution can have a profound influence on the long-range magnetic structure.

In this study, we measure the dynamics of the inner shell f-electron spin helix in Dysprosium in response to transient injection of conduction electrons with unpolarized spins. We

observe a reduction in the amplitude of the helical order parameter and a shift in the helical wavevector q on disparate time-scales that are strongly dependent on both pump fluence and sample temperature. Measurements of the ferromagnetic (FM) phase dynamics is consistent with FM phase measurements of Lanthanide metals such as Tb and Gd, where the dynamics of the core and conducting spins occur on ps timescales [5, 6, 8]. Notably, the dynamics in the helical antiferromagnetic phase (HAF) of Dy are significantly slower, with characteristic time-scales of tens of picoseconds. We attribute these anomalous dynamics to the relationship between the wave vector of the conduction level electronic excitation $k$ and the wave vector of the core magnetic ordering $q$. In the FM phase, the electronic excitation at $k = 0$ is closely coupled to the magnetic ordering at $q = 0$. In the HAF phase, the core spin helix is concomitant with a nesting of the Fermi surface (FS). Initial ultrafast scattering of spins from the $k = 0$ excitation does not directly change the energy-minimizing configuration of the system, and instead the helical dynamics are driven by changes to the shape of the FS and subsequent changes to the electron distribution through scattering events.

Magnetization dynamics were investigated in an epitaxially grown yttrium(Y)/dysprosium(Dy)/yttrium(Y) (20/500/20 nm) multilayer film that exhibits a second-order phase transition to a helical antiferromagnetic phase below $T_N$ = 180 K [9]. A magnetostriction driven first order transition to a ferromagnetic phase occurs at $T_C$ = 60 K, where $T_C$ is reduced relative to the bulk due to strain induced by the underlying yttrium layer. Between $T_N$ and $T_C$, the pitch of the spin helix, $\theta = qa$ (where a is the lattice constant), changes continuously with temperature, from 46 degrees (q=2.24 nm$^{-1}$) at $T_N$ to 30 degrees (q=1.46 nm$^{-1}$) at $T_C$ [10].

## EXPERIMENTAL RESULTS

### Ultrafast Optical Measurements

Dynamics of the low-temperate FM phase were observed using magneto-optical Kerr measurements. The photo-induced change in reflectivity (dR/R) and magnetooptic Kerr (MOKE) angle ($d\theta$) for the Y/Dy/Y stack are shown in figure 1. The reflectivity and MOKE measurements were recorded using 100 fs pulses with a probe energy of 3.0 eV and an excitation energy of 1.5 eV. These measurements were performed in a polar geometry with an applied field of 0.5 T perpendicular to the sample surface. The reflectivity signal shows multiple time-scale dynamics within 2 ps, which we attribute to reflections from the front surface and the top Y/Dy interface. The ($d\theta$) dynamics show a rise time of $\sim$ 300 fs. Both signals show a recovery time of 2.5 ps and a remnant excitation beyond 10 ps.

The MOKE signal shows a clear change in amplitude at the ferromagnetic transition temperature. This change occurs within 1 ps, indicating that the 1.5 eV optical pulse excites the conduction-level magnetism on time-scales similar to those observed in previous ultrafast measurements of lanthanide magnets [1, 5–8]. A sharp change in amplitude at $T_C$ is not observed in the reflectivity measurements. Dynamics of the MOKE signal continue above $T_C$ in the AFM and paramagnetic phases, which we attribute to dynamics of the field-canted out-of-plane magnetic moment.

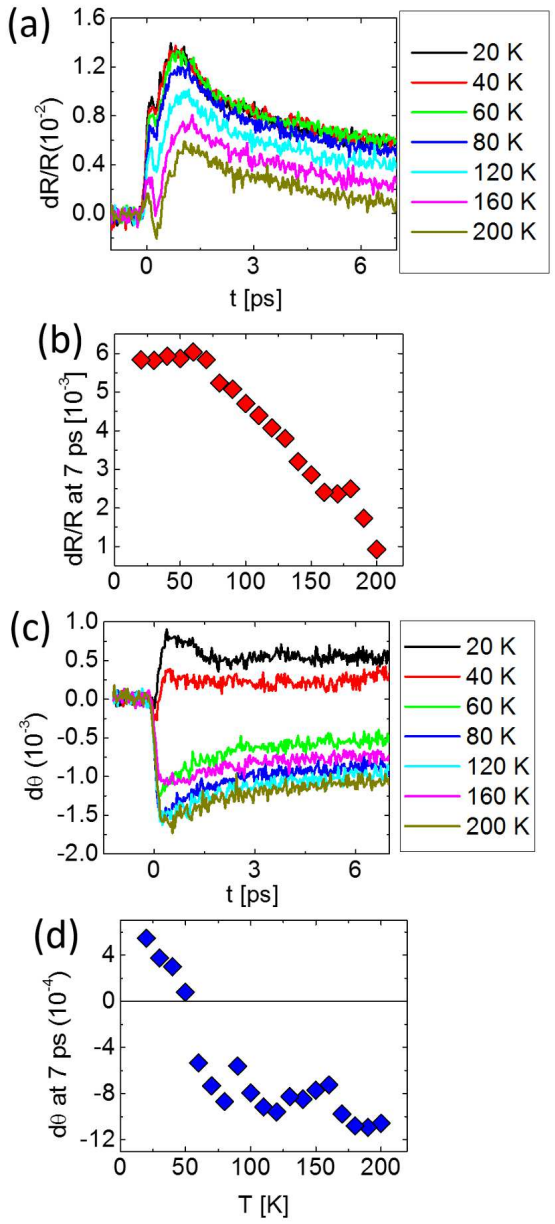


FIG. 1. Optical pump-probe data of the Y/Dy/Y thin film. (a) dR/R as a function of temperature from 20 K (top, purple) to 200 K (bottom, black). (b) Temperature dependence of the dR/R amplitude (c) $d\theta_K$ as a function of temperature from 20 K (top, purple) to 200 K (bottom, black). (d) Temperature dependence of the amplitude of $d\theta_K$.

The 20 nm top Y layer absorbs $\sim 90$ % of the pump energy, creating a hot electron distribution in the Y layer and resulting in ultrafast injection of unpolarized spins into the 500 nm Dy film via nonequilibrium diffusion [5, 6, 11]. The MOKE measurements indicate an ultrafast excitation of the conduction level spins, resulting from sub-ps injection of hot unpolarized electrons from the Y layer and consistent with dynamics observed for the same process in other magnetic materials [5, 6, 11].

### Resonant Scattering Measurements

Dynamics in the helical phase were probed using resonant x-ray scattering, which provides a direct probe of the core-spin helical ordering through direct optical transitions between atomic core levels and the valence f-orbital [10]. As in the MOKE measurements, the sample is excited with an optical pump pulse with a photon energy of 1.5 eV and a duration of 100 fs. Time-resolved diffraction measurements were performed at beamline 6.0.2 at the Advanced Light Source, Lawrence Berkeley National Laboratory, utilizing a probe energy of 1290 eV, resonant with the Dy M5-edge, with a probe pulse duration of 70 ps.

Figure 2 shows the spiral diffraction peak with a pump fluence of 0.66 mJ/cm$^2$ at 105 K as a function of pump-probe time delay. The dynamics of the diffraction peak, consisting of the onset of the excitation and subsequent recovery, are faster than the corresponding shifts in scattering wavevector. The initial response of the helix is characterized by a reduction of diffraction intensity (I) occurring on a 200 ps time scale, and an increase of the peak wave-vector (q) occurring on a 1 ns time scale. Both q and I recover on time scales of several ns. The parameters I and q are determined by fitting the measured rocking curve with a Lorenztian function. The diffraction peak corresponds to the periodicity of the helix perpendicular to the plane of the film, and we observe no change in the rocking curve width within the accuracy of the fits ($\sim 2\%$), which is likely limited by the 30 nm penetration depth of the x-ray probe. There is also no observable change in the diffraction peak width that would indicate a change in the in-plane domain structure, and the dynamics of the diffraction signal can therefore be completely characterized by I(t) and q(t).

Figure 3 shows the time-dependence of I and q as a function of pump fluence at 105 K. The excitation and recovery dynamics become slower with increased fluence for both the parameters. The maximum reduction in the diffraction intensity ($\delta I/I_0$) is linear with fluence. The shift in wavevector shows a saturation-like behavior at early time delays with fluences above 1.5 mJ/cm$^2$ and is linear with fluence for delays $>$ 20 ns. The slow dynamics of the core spin spiral is in stark contrast with the ultrafast MOKE measurements of the conduction-level magnetism.

On long time-scales ($>$ 20 ns), the changes in the diffraction peak are consistent with a uniform increase in the sample temperature. As the sample is cooled from from $T_N$ to $T_C$, static measurements show a monotonic decrease in q with little variation in the diffraction efficiency at intermediate temperatures[10]. Thus on a 20 ns time scale both I and q can be parameterized by an increase in the sample temperature $T$, such that the magnetic state described by $I(T), q(T)$ maps onto measured static values. The increase in q-vector with fluence is shown in figure 3(c) at 105 K. The linear dependence on fluence is expected for a regime in which the specific heat is roughly constant with photo-induced change in temperature: $dT = dE/C(T) \sim dE/C$, where $C$ is the specific heat and $dE$ is the energy deposited by the pump pulse. The max-

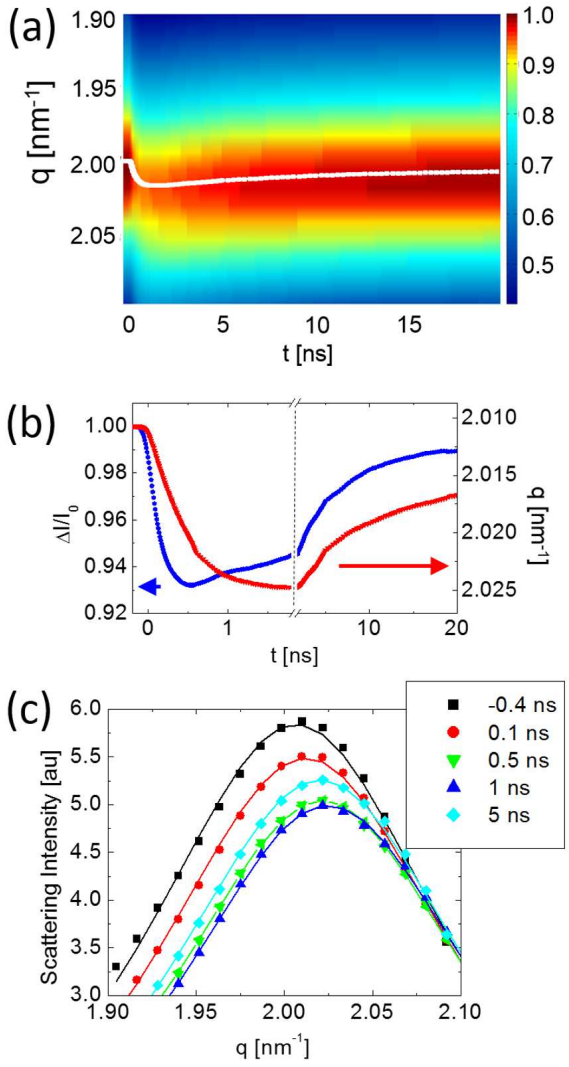


FIG. 2. (a) Colormap of the diffraction peak intensity as a function of time delay, recorded by scanning time-delay at different scattering wave-vectors. The white line indicates the time-dependence of the scattering wave vector. (b) Scattering peak intensity (blue curve, left axis) and wave vector (red curve, right axis) as a function of time delay for data in panel (a). Note that the axis of the wave vector in (a) and (b) has been inverted to accommodate comparison of the $I$ and $q$ dynamics. (c) Rocking curve scans at different time delays. Solid lines represent fits with fixed rocking curve width.

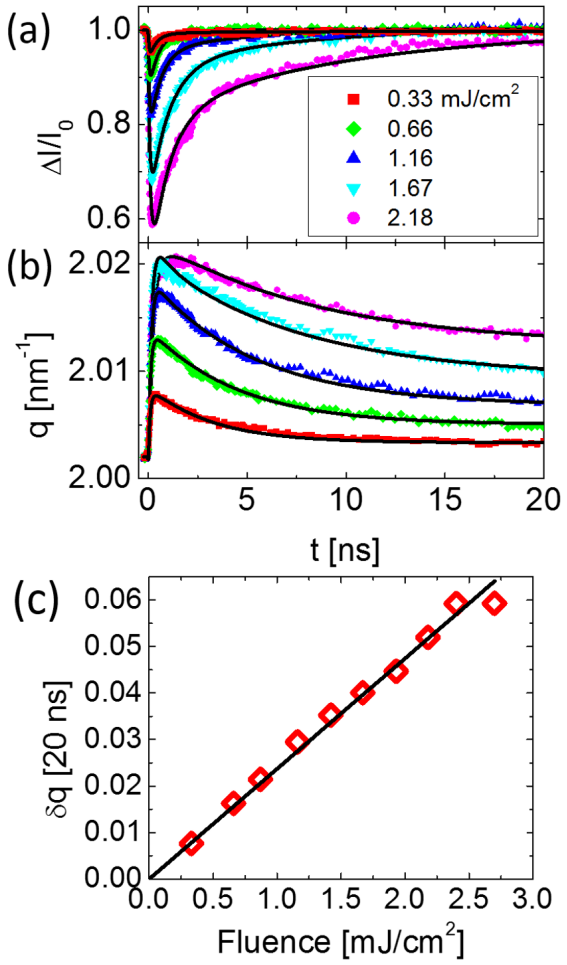


FIG. 3. Time-dependence of the loss in diffraction peak intensity (a) and change in q-vector (b) as a function of pump fluence. Solid lines indicate fits to the model described in the text. (c) Remnant change in q as a function of pump fluence showing linear dependence consistent with sample heating.

imum temperature increase is $\sim$ 5 K at the highest fluence. Thermal lattice changes can also be eliminated as the cause of the time-dependent shift in $q$. The lattice constant along the spiral direction is reduced by $\delta c/c = 0.003$ as the sample is heated through the helical phase, making the observed shifts in the magnetic wavevector $q$ with laser excitation too large to be attributed to a thermal change in the lattice constant [9].

At times shorter than $\sim$ 20 ns, the large transient photo-induced reduction in I, coupled with only a moderate increase in q, is not consistent with any statically measured magnetic configuration, and indicates that the dynamics observed on time-scales faster than $\sim$ 20 ns cannot be described by an increase in the sample temperature. Specifically, by comparing the time-resolved data with static temperature dependent measurements of the rocking curve, the shape of the rocking curve cannot be characterized by $I(T)$, $q(T)$, and a time-dependent temperature these timescales. The spiral wave-vector remains uniform throughout the probed region, as indicated by the constant rocking curve width, and indicates that spatial inhomegeneities in the excitation region are not responsible for the observed changes in the diffraction peak.

Figure 4 shows the temperature dependence of the spin-ordering peak dynamics. Both the onset and recovery of the $q$ shift become progressively slower with increasing temperature. The dynamics of $\delta I/I$ show a less dramatic slowing with temperature. The maximum shift in $q$ is non-monotonic with temperature, with a maximum shift at 90 K. The photo-induced reduction in $I$ shows little dependence on temperature, except near $T_N$, as shown in figure 4.

## DISCUSSION

The microscopic origin of the HAF dynamics is clarified by considering the relationship between the core spin ordering and the conduction electron FS. In equilibrium, the FS has extended regions in which electrons can scatter from $\phi(k)$ to $\phi(k+q)$, which combined with the exchange interaction between core and conduction spins, leads to helical ordering of the core spins with wave vector q [12]. The temperature dependence of q results primarily from the dependence of the helical ordering energy gap on thermal fluctuations of the basal plane magnetization, leading to a re-shaping of the FS as the thermal fluctuations are frozen out [13–16].

In the spiral phase, the 1.5 eV excitation generates hot electrons, creating an excitation at $k = 0$ in the conduction spins and perturbing the conduction-level magnetic ordering while preserving the FS nesting q. The induced disorder of the conduction spins reduces the number of quasi-elastic $k \rightarrow k+q$ scattering events where spin angular momentum is conserved, and increases $k \rightarrow k+q$ scattering involving changes in angular momentum. The core/conduction exchange couples this angular momentum scattering to the core helix, propagating spin disorder to the core spins, but not initially changing the favored helical wave-vector.

The response of the core-spins to the perturbed conduction electron distribution mimics the reduction in the magnetization due to thermal excitations, and the equilibrium wave vector q for the FS nesting and core helix changes due to the dependence of q on the basal plane magnetization. This process is diagrammed in figure 5. The shift in the nesting vector of the FS creates a mismatch between the FS and the electron distribution. The electron distribution relaxes via inelastic scattering events that couple electrons with excess energy (above $\mathrm{E}_{Fermi}$) with hole states below $\mathrm{E}_{Fermi}$, with transfer of spin angular momentum occurring through exchange and spin-orbit coupling interactions. This situation is analogous to the breathing Fermi surface model used to describe damping of the precession in ferromagnets, in which the dynamical pointing of the ferromagnetism alters the FS through spin-orbit coupling [17–19]. The excitation time-scales observed in the helical system are similar to damping time-scales in other magnetic systems, limited by the scattering rate and efficiency of angular momentum transfer during scattering events.

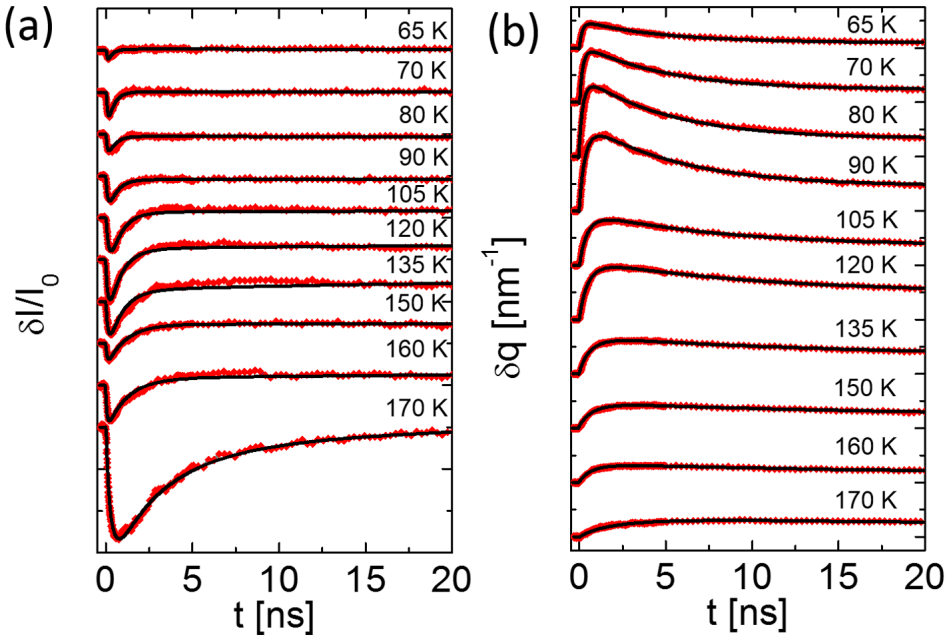


FIG. 4. Temperature dependence of (a) $\delta I/I$ and (b) wavevector ($q$) for a pump fluence of 0.66 mJ/cm$^2$. Lines are fits from the GP model described in the text.

## MODEL

For non-thermal dynamics in magnetic systems, the three temperature model (3TM) is often invoked to describe the dynamics in terms of energy transferred between electronic, lattice, and spin degrees of freedom, with laser-induced disorder in the spin system modeled as an increase in spin temperature $T_S$ [1, 20, 21]. In a ferromagnet, this spin temperature defines the state of a global, uniform magnetization. In the HAF phase of Dy, the magnetic state is defined by both the strength of the order parameter and the helical wavevector, and the electronic configuration and helical ordering are interdependent through nesting of the FS. A model with single effective spin temperature and the parameterization $I(T_S), q(T_S)$ fails to describe the short time-scale dynamics, as discussed above, as a single spin temperature cannot account for both parameters of the magnetic configuration. While the 3TM includes a phenomenological treatment of the core spin/conduction electron coupling, it does not naturally account for the effect of this coupling on the shape of the FS and the closely related helical spin configuration.

Instead, we employ a Gross-Pitaevski (GP) model, which models the dynamics through motion of a free energy surface, phenomenologically accounting for both the coupled magnetic state parameters I and q and changes to the shape of FS [22, 23]. We use this model to derive changes to the exchange constants which are consistent with the ultrafast dynamics measured in figure 2. We use a Hamiltonian given by

$$H = \frac{J_1}{2a}\int d^3x \left[-\frac{\theta}{2}\left(\nabla m\right)^2 + \frac{a}{4}\left(\nabla^2 m\right)^2\right], \qquad (1)$$

where $m$ is the strength of the order parameter of the HAF, proportional to the experimentally measured I. This Hamiltonian contains the exchange terms $J_1$ and $J_2$, which are the effective nearest and next-nearest neighbor coupling between core spins that stabilize the helical phase. $J_2$, appears through $\theta$, which is the equilibrium turn angle of the helix given by $cos(\theta) = J_1/4J_2$. The helix is the lowest energy state of this system when $J_1$ and $J_2$ have opposite sign.

For a one-dimensional helical magnetic structure with wave-vector $q$, the above Hamiltonian leads to an effective free-energy given by:

$$F = -m^2\alpha\left(T\right) + \beta m^4 + \frac{1}{2}J_1 a^2 m^2\left(-\frac{\theta^2 q^2}{2} + \frac{a^2 q^4}{4}\right) \qquad (2)$$

.

The first two terms, with factors $\alpha$ and $\beta$, are the lowest-order terms in the free energy expansion that stabilize the order parameter for $T < T_N$, and $a$ is the lattice constant. Changes to the free energy of the core helix arising from excitation of the conduction electrons are considered through the parameters $J_1$ and $J_2$ . Note that $\theta$ and $q$ are retained as variables to distinguish the equilibrium helix turn angle from the measured dynamic variable q.

The dynamics can be calculated by using the Hamiltonian to describe an effective action of the helical system parameterized by $m$ and $q$. From equation 2, we can write the equations of motion as

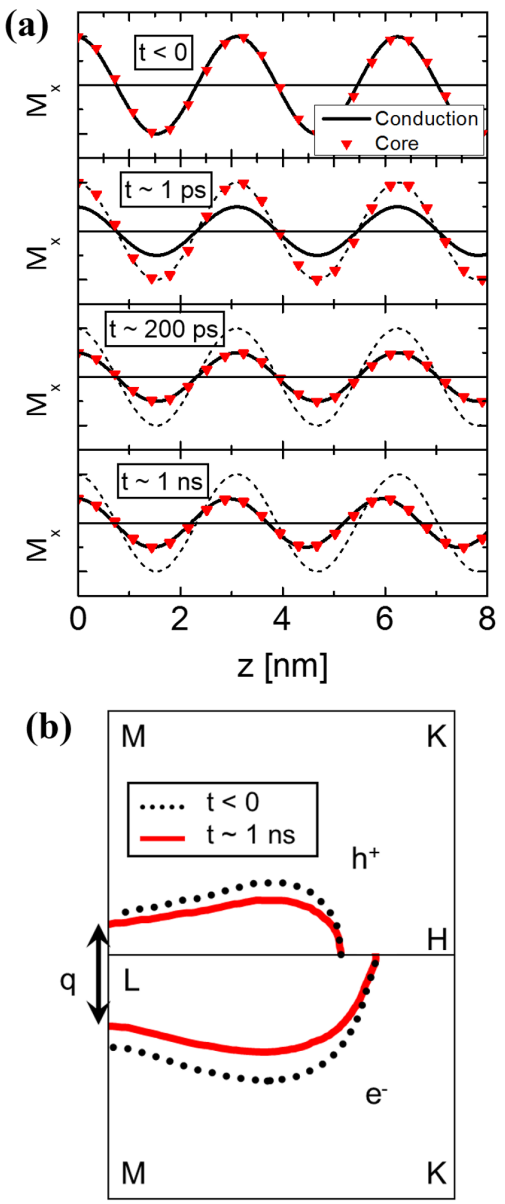


FIG. 5. (a) Diagram of real-space spin ordering of core and conduction electrons for a spiral with $q \| z$. The y-axis units are arbitrary. (t < 0) Equilibrium distribution (t ∼ 1 ps) Photoexcitation of conduction electrons, followed by (t ∼ 200 ps) excitation of core spins, and (t ∼ 1 ns) subsequent shift in q. The dotted lines show the equilibrium distribution for reference. (b) Corresponding FS diagram. Adapted from [12]

$$\gamma_m \dot{m} = 2\alpha m - 4\beta m^3 - J_1 m a^2 \left( -\frac{q^2\theta^2}{2} + \frac{a^2 q^4}{4} \right) \quad (3)$$

$$\gamma_q \dot{q} = -\frac{1}{2} J_1 m^2 a^2 q(-\theta^2 + a^2 q^2). \quad (4)$$

Due to the absence of oscillations in the data, we neglect the second derivative terms in the above equation. Additionally, we have introduced phenomenological damping terms with parameters $\gamma_m$ and $\gamma_q$ to account for relaxation of the system back to equilibrium.

The behavior of $m$ and $q$ with different rheonomic constraints provides insight into the origins of the dynamics of the spin helix. Within the GP model, the dynamics of the parameters $J_{1,2}$ emulate the dynamics of the FS, and the damping parameters model the scattering mechanisms that drive the spin-ordering to match the FS. The observed dynamics I and q are described by introducing time-dependent parameters $J_1(t)$ and $J_2(t)$ into equations 3 and 4 such that the derived $m$ and $q$ match the data.

We choose $J_1(t)$ and $J_2(t)$ to be consistent with our microscopic picture in the following ways. The uniform (k = 0) excitation of the conduction electrons is modeled as a proportional reduction in both exchange parameters, such that initially the equilibrium q-vector is unchanged. We introduce two recovery time-constants to describe the observed recovery times in the data, and we introduce parameters $\sigma$ and $\rho_2$ to account for the symmetric and asymmetric recovery amplitudes of the exchange constants. Within this model, the exchange parameters vary according to

$$\frac{\delta J_1(t)}{J_1(0)} = \delta J_{init}((1 - \sigma - \delta J_{T,1})e^{-t/\tau_a} + \sigma e^{-t/\tau_b} + \delta J_{T,1}) \quad (5)$$

$$\frac{\delta J_2(t)}{J_2(0)} = \delta J_{init}((1 - \sigma - \rho_2)e^{-t/\tau_a} + \sigma e^{-t/\tau_b} + \rho_2 e^{-t/\tau_2}). \quad (6)$$

The onset of the reduction in $J_{1,2}$ is instantaneous to be consistent with observed optical MOKE data in figure 1, and the slow onset of the reduction in $m$ is limited by the damping parameter $\gamma_m$. Shifts in $q$ are treated as partial asymmetric recoveries of either exchange parameter. The black lines in figure 3 show fits to the data using $m(t)$ and $q(t)$ calculated with the GP model.

Figure 6 (a) shows the initial reduction in the exchange parameters $\delta J_{init}$ and the recovery amplitude $\sigma$. The initial reduction in the exchange is linear with fluence, as would be expected from an effective exchange proportional to the spin ordering and an injected unpolarized spin population that scales with the fluence. The initial change in the exchange constants are equal for $J_1$ and $J_2$ and therefore do not lead to a shift in the spiral wavevector. The time-scales for the recovery, $\tau_a$ and $\tau_b$ are shown in figure 6 (b).

The initial shift in $q$ occurs through a relatively fast recovery of $J_2$ through the term $\rho_2$. This parameter is shown in figure 6 (c). The shift in q for time delays greater than 20 ns is treated through $J_{T,1}$, which is a small remnant reduction in $J_1$ representing an increased sample temperature. Note that $\{J_{T,1}, \rho_2\} \ll \{\delta Ji, \sigma\}$; the terms representing antisymmetric dynamics in $J_1$ and $J_2$ that shift the spiral $q$ are much smaller than the symmetric changes in the exchange constants, resulting in overall dynamics of $J_1$ and $J_2$ that are nearly symmetric.

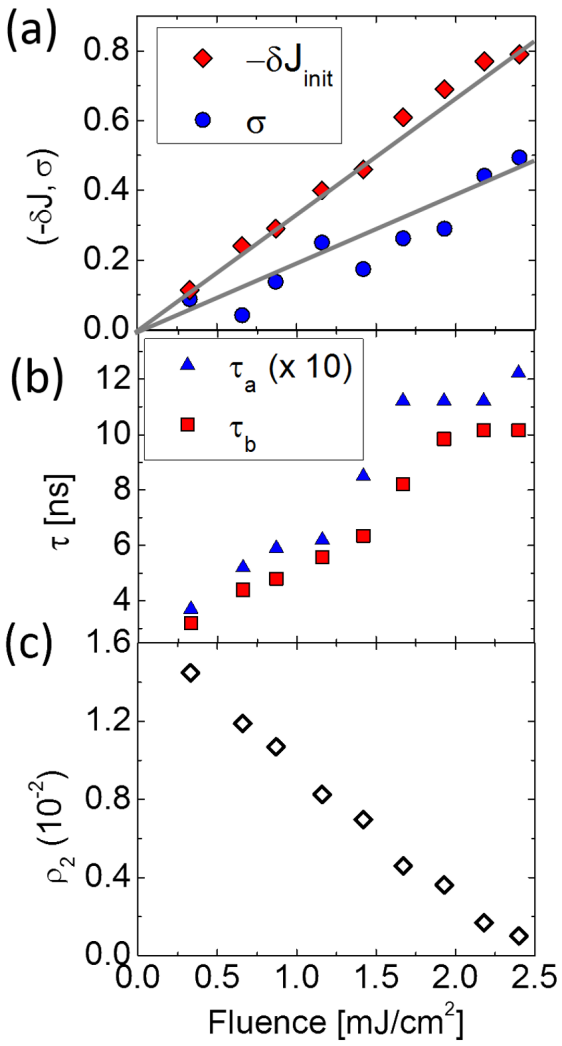


FIG. 6. Magnitudes and time-scales of changes in exchange parameters $J_1$ and $J_2$ used to describe the fluence dependence of the data. (a) Amplitudes of initial reduction and proportional recovery of the exchange parameters. Note $\delta J_{init}$ is negative, and the line indicates a linear reduction in the exchange parameters with fluence. (b) Proportional recovery timescales. (c) Non-proportional recovery in $J_2$ leading to the shift in $q$. $\rho_2$ becomes smaller with fluence, leading to saturation-like behavior for the shift in spiral wavevector.

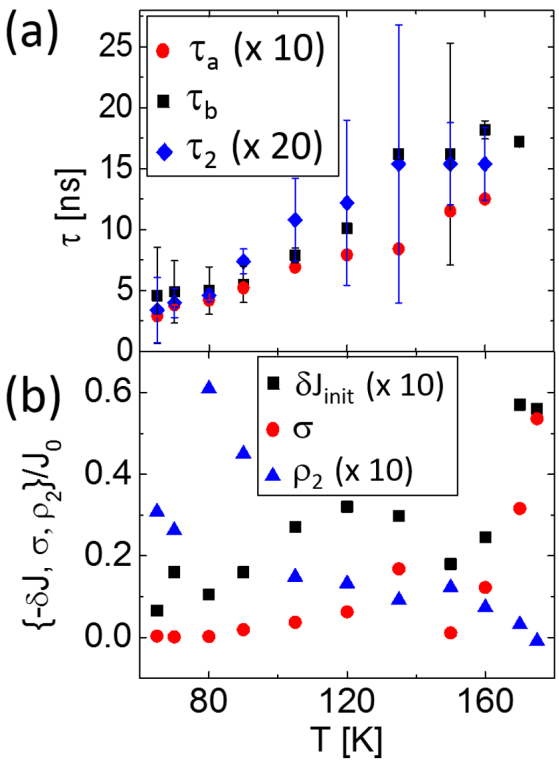


FIG. 7. (a) Time-scales of exchange parameters $J_1$ and $J_2$ as a function of temperature. (b) Reduction amplitudes of $J_1$ and $J_2$ as a function of temperature.

The modeled time-constants become slower with increasing fluence (figure 6(b)) and also become slower as T is increased from $T_C$ to $T_N$ as shown in figure 7(a). Both of these trends suggest a link between the magnetic ordering and the recovery time-scales of the spin helix. Figure 7(b) shows the temperature dependent changes in $J_1$ and $J_2$, with increases in the symmetric parameters near $T_N$ corresponding to softening of $J_1(0), J_2(0)$ near the transition temperature. The combined fluence and temperature dependence of the time constants is consistent with changes in the shape of the FS, with a corresponding reduction in the effective exchange coupling between core spins, resulting from a reduction of the basal plane magnetization $m$ [13–16].

Moreover, the GP model adequately describes the $\delta I/I$ temperature dependence in figure 4a, which shows an increase in scattering signal on time-scales of $\sim 10$ ns for intermediate temperatures. This results from the relatively slow damping of the spiral wavevector to the pseudo-equlibrium excited value and a relatively large change in $\theta$ relative to the change in $J_1$. From 2, the equilibrium $m$ is related to $q$ and $\theta$ by:

$$m_0 = \sqrt{\frac{J_1 a^2 q^2 \left(2\theta^2 - a^2 q^2\right) + 8\alpha}{16\beta^2}}. \qquad (7)$$

The equilibrium turn angle $\theta$ is increased by the laser excitation, which leads to a larger difference $\theta$ and $aq$ and an increase in $m_0$. This increase will appear in the dynamic parameter $m$ whenever $J_1$ and $\theta$ reach pseudo-equilibrium excited values and $m$ damps quickly relative to the damping time of $q$.

The equilibrium helical phase results from the interaction between the core spins and the nested FS of the conduction electrons; the phenomenological GP model provides a shorthand to account for dynamics of the nested FS through $J_{1,2}$ and subsequent electron population scattering events through $\gamma_{m,q}$. By considering changes to the shape of the free energy surface, the GP model provides an accurate description of the helical motion with fluence and temperature dependence that is qualitatively consistent with both the static and optical dy-

namic measurements. We observe a linear reduction in the exchange coupling with laser fluence, indicating a direct excitation of the conduction electrons, and fluence and temperature dependence of the recovery time scales consistent with an effective exchange coupling that scales with $m$.

In summary, the dynamics of the helical phase in response to transient unpolarized spin injection differ significantly from those in the ferromagnetic phase due to the relationship between the core spins and conduction electron FS nesting. FM phase dynamics result from close coupling of the $k = 0$ excitation to the core spins through spin-orbit coupling and short range exchange interactions. The dynamics of the helical phase result from indirect excitation to the finite wave-vector ordering through a fundamentally different process, analogous to a damping mechanism, that transfers angular momentum between the excited conduction electrons and core spins.

The work at LBNL, including experiments at ALS, was supported by the Director, Office of Science, Office of Basic Energy Sciences, of the U.S. Department of Energy under Contract No. DEAC02-05CH11231.

[1] A. Kirilyuk, A. V. Kimel, and T. Rasing, Rev. Mod. Phys. **82**, 2731 (2010).
[2] S. Mathias, C. La-O-Vorakiat, P. Grychtol, P. Granitzka, E. Turgut, J. Shaw, R. Adam, H. Nembach, M. Siemens, S. Eich, C. Schneider, T. Silva, M. Aeschlimann, M. Murnane, and H. Kapteyn, PNAS **109**, 4972 (2012).
[3] I. Radu, K. Vahaplar, C. Stamm, T. Kachel, N. Pontius, H. A. Dürr, T. Ostler, J. Barker, R. Evans, R. Chantrell, A. Tsukamoto, A. Itoh, A. Kirilyuk, T. Rasing, and A. Kimel, Nature **472**, 205 (2011).
[4] B. Coqblin, *The Electronic Structure of Rare Earth Metals and Alloys* (Academic Pr, 1978).
[5] M. Wietstruk, A. Melnikov, C. Stamm, T. Kachel, N. Pontius, M. Sultan, C. Gahl, M. Weinelt, H. A. Dürr, and U. Bovensiepen, Phys. Rev. Lett. **106**, 127401 (2011).
[6] R. Carley, K. Döbrich, B. Frietsch, C. Gahl, M. Teichmann, O. Schwarzkopf, P. Wernet, and M. Weinelt, Phys. Rev. Lett. **109**, 057401 (2012).
[7] M. Lisowski, P. A. Loukakos, A. Melnikov, I. Radu, L. Ungureanu, M. Wolf, and U. Bovensiepen, Phys. Rev. Lett. **95**, 137402 (2005).
[8] A. Eschenlohr, M. Sultan, A. Melnikov, N. Bergeard, J. Wieczorek, T. Kachel, C. Stamm, and U. Bovensiepen, Phys. Rev. B **89**, 214423 (2014).
[9] K. Dumesnil, A. Stunault, P. Mangin, C. Vettier, D. Wermeille, N. Bernhoeft, S. Langridge, C. Dufour, and G. Marchal, Phys. Rev. B **58**, 3172 (1998).
[10] S.-W. Chen, H. Guo, K. A. Seu, K. Dumesnil, S. Roy, and S. K. Sinha, Phys. Rev. Lett. **110**, 217201 (2013).
[11] M. Battiato, K. Carva, and P.M. Oppeneer, Phys. Rev. Lett. **105**, 027203 (2010).
[12] S. C. Keeton and T. L. Loucks, Phys. Rev. **168**, 672 (1968).
[13] R. Elliott and F. Wedgwood, Proc. Phys. Soc. **81**, 846 (1963).
[14] R. Elliott and F. Wedgwood, Proc. Phys. Soc. **84**, 63 (1964).
[15] K. Yosida and A. Watabe, Progress of Theoretical Physics **28**, 361 (1962).
[16] K. M. Döbrich, A. Bostwick, J. L. McChesney, K. Rossnagel, E. Rotenberg, and G. Kaindl, Phys. Rev. Lett. **104**, 246401 (2010).
[17] V. Kamberský, Can. J. Phys. **78**, 2906 (1970).
[18] M. Fähnle and D. Steiauf, Phys. Rev. B **73**, 184427 (2006).
[19] D. Steiauf, J. Seib, and M. Fähnle, Phys. Rev. B **78**, 020410 (2008).
[20] T. Ogasawara, K. Ohgushi, Y. Tomioka, K. S. Takahashi, H. Okamoto, M. Kawasaki, and Y. Tokura, Phys. Rev. Lett. **94**, 087202 (2005).
[21] B. Koopemans, G. Malinowski, F. Dalla Longa, D. Steiauf, M. Fähnle, T. Roth, M. Cinchetti, and M. Aeschlimann, Nature Materials **9**, 259 (2010).
[22] F. Li, T. Nattermann, and V. L. Pokrovsky, Phys. Rev. Lett. **108**, 107203 (2012).
[23] E. Gross, Nuevo Cimento **20**, 454 (1961).